

# Trapped fireshell (halo) of photons and pairs around black-hole horizon: source for ultra-high-energy particles

**She-Sheng Xue**

ICRANet Piazzale della Repubblica, 10 -65122, Pescara, Italy  
 Physics Department, Sapienza University of Rome, Rome, Italy  
 INFN, Sezione di Perugia, Perugia, Italy  
 ICTP-AP, University of Chinese Academy of Sciences, Beijing, China  
 E-mail: [xue@icra.it](mailto:xue@icra.it), [she-sheng.xue@cern.ch](mailto:she-sheng.xue@cern.ch)

**Abstract.** We study the Compton-rocket effect of multi-photon interacting with electrons in an opaque fireball (or fire spot) of photons and  $e^-e^+$  pairs at temperature  $T_\gamma \gg m_e$ . We find the charged-particle acceleration and the avalanche runaway process, leading to a non-trivial probability of ultra-high-energy (UHE) electrons and protons, which subsequently produce very-high-energy (VHE) photons and neutrinos. We show such peculiar dynamics using the Gamma-Ray Burst central engine fireball, whose inner part inflows and forms a gravitationally trapped fireshell (halo) around a black hole. The halo is a metastable, cooling via UHE particle emissions and black-body radiation. We calculate the UHE particle luminosity varying in time, and discuss the peculiar features of such produced UHE particles, which lead to VHE particles, in connection with possible numerical simulations, observations and experiments.

---

## Contents

<b>1</b>	<b>Introduction</b>	<b>2</b>
<b>2</b>	<b>Trapped fireshell (halo) around black hole horizon</b>	<b>2</b>
2.1	Tolman–Oppenheimer–Volkoff equation for halo energy density	3
2.2	Thermodynamic and opaque fluid of photons and pairs	5
<b>3</b>	<b>Compton-rocket effect on accelerating electrons</b>	<b>7</b>
3.1	Optically thin plasma of electrons and protons irradiated by photons	7
3.2	Electrons and protons in an opaque fluid of photons and pairs	8
3.3	Drifting electrons in an opaque fluid of photons and pairs	9
<b>4</b>	<b>Runaway electrons in an opaque fluid photons and pairs</b>	<b>10</b>
4.1	Accelerated electron runaway due to Klein–Nishina corrections	10
4.2	Electrons accelerated by photons and pairs at high temperature	11
4.3	Superthermal spectrum of UHE electrons	12
4.3.1	Thomason scattering in low energies	12
4.3.2	Klein–Nishina scattering in high energies	14
4.4	Runaway protons pulled by runaway electrons	16
<b>5</b>	<b>Luminosities of UHE particles and blackbody radiation</b>	<b>17</b>
5.1	Blackbody radiation luminosity and MeV annihilation line	18
5.2	UHE emission luminosity and energy spectrum	18
5.3	UHE emission luminosity and halo temperature decrease in time	20
<b>6</b>	<b>Characteristics relevant for observations and experiments</b>	<b>22</b>
6.1	Peculiar features of the mechanism accelerating UHE particles	22
6.2	Possible relevance for observations and experiments	23

---

# 1 Introduction

The discovery of ultra-high-energy (UHE  $\sim 10^{18-20}$  eV) charged particles (cosmic rays) has been for decades. The acceleration mechanism of UHE charged particles remains mysterious, although much theoretical and observational progress has been made to understand their nature and identify their sources (see review [1]). Very-high-energy (VHE  $\sim 10^{12-15}$  eV) neutral particles (photons and neutrinos) have been recently observed by the LHAASO [2], MAGIC [3] and ICECUB [4] collaborations. Much theoretical attention has been given to understanding the origin of VHE neutral particles. In principle, the primary UHE charged particles are energetic enough to produce secondary VHE neutral particles. Thus, two highly energetic particle events may correlate and originate from compact and powerful astrophysical sources, such as gravitational accretion disks, massive collapses, binary coalescence and active galactic nuclei. In these arenas, strong radiation fields and charged particles non-linearly interact via the Compton rocket effect [5–7] on relativistic electrons by the anisotropy of multi-photons and electron scattering. This dynamics has been studied by particle-in-cell numerical simulations [8–11].

One of these powerful astrophysical sources can be the central engine for Gamma-ray bursts (GRBs), an opaque fireballs of large ultra-relativistic particle energy density and pressure [12], and see reviews [13–20]. Within the general relativity (GR) framework, we studied [21, 22] the hydrodynamical outflow of fireballs by using also the Boltzmann rate equation for electrons and positrons (pairs) annihilation to photons, obtaining the relation between the photon heat and baryon kinetic energies for main bursts and afterglow radiations. Further scrutiny study [23] shows in Fig. 1 that the fireball’s inner part is trapped due to strong gravitational attraction, prevailing over thermal pressure repulsion. On the contrary, its outer part outflows, accounting for the GRB phenomenon. The separatix between the inner and outer parts is  $\bar{R} \approx 4GM = 2r_+$  near the horizon.

We will show in Section 2 that through the gravitational and thermal forces’ equilibrium, the trapped fireball’s inner part (halo around a black hole) forms a metastable thermal fluid of photons and pairs at high energy density and temperature. Using such an opaque horizon halo as an example, we study the Compton-rocket effect on accelerating charged particles (Section 3) and the avalanche runaway process (Section 4) leading to UHE electrons and protons. We calculate the luminosity of UHE particles and the halo cooling in Section 5, and discuss the peculiar features of UHE and VHE particles produced in this dynamics, in connection with numerical simulations, observations, and experiments in the final Section 6.

## 2 Trapped fireshell (halo) around black hole horizon

The highly energetic and dense fireshell comprises ultra-relativistic particles and antiparticles, for example, photons  $\gamma$ , electrons  $e^-$  and positrons  $e^+$  pairs, undergoing the back and forth process  $\gamma + \gamma \leftrightarrow e^+ + e^-$ , which establishes a local thermal equilibrium at high temperatures. We describe the fireball as a perfect fluid of energy density  $\rho_\gamma(r)$

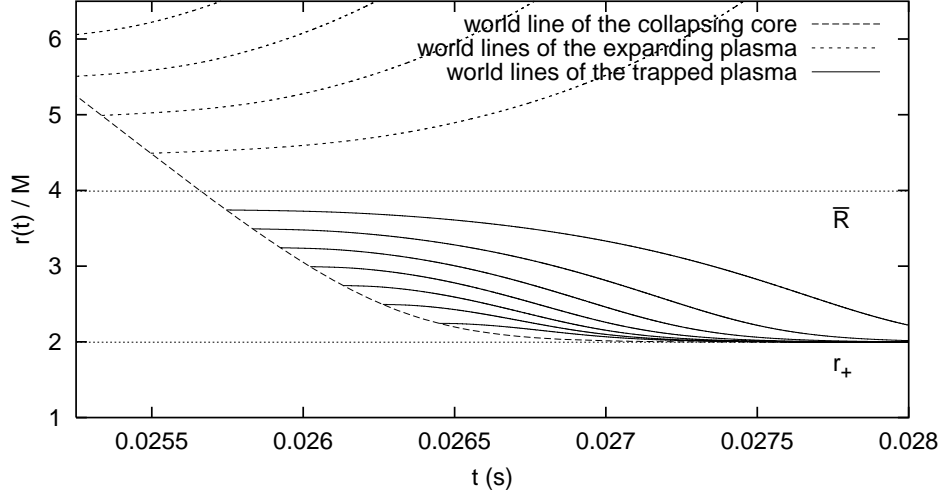


**Figure 1.** Figure 2 of Ref. [23] shows the world lines of fireball hydrodynamics expanding outflow (dot line) and trapped inflow (solid line) in the Schwarzschild geometry of a collapsing core (dashed line) of the mass  $M$ , and horizon radius  $r_+ = 2M$ . The separatrix radius between out and in flows is  $\bar{R} = 4M$ , and the trapped inflow energy is about half of the expanding outflow energy. We can approximately obtain the separatrix by estimating the balance between thermal repulsive pressure and gravitational attractive force  $4\pi r_+^2 \rho_\gamma(r_+) c \sim Gm_\gamma M/r_+^2$  on the photon-pair shell of mass energy  $m_\gamma = \rho_\gamma(r_+) 4\pi r_+^2 \bar{R}$ . It is in distinct contrast with the processes of pressure-less baryon dust or a test particle free-falling in a gravitational collapse. The gravitational time dilation  $\delta t = \left(1 - \frac{2Gm(r)}{r}\right)^{-1/2} \delta\tau \rightarrow \infty$  for an observer at infinity is evident near the horizon  $r \rightarrow r_+$ , and  $\delta\tau$  is a finite proper time (distance) for a local observer.

and pressure  $P_\gamma(r)$  with the Equation of State  $P_\gamma(r) = \rho_\gamma(r)/3$ . Baryonic matter is ionised, and its amount and binding energy are negligible in studying fireballs at high temperatures.

## 2.1 Tolman–Oppenheimer–Volkoff equation for halo energy density

We adopt the spherically symmetric Tolman–Oppenheimer–Volkoff (TOV) equation to study the gravitational equilibrium configuration of ultra-relativistic photons and electron-positron pairs trapped by the gravitational force near the horizon,

$$\frac{dP_\gamma}{dr} = -\frac{Gm(r)}{r^2} \rho_\gamma \left(1 + \frac{P_\gamma}{\rho_\gamma}\right) \left(1 + \frac{4\pi r^3 P_\gamma}{m(r)}\right) \left(1 - \frac{2Gm(r)}{r}\right)^{-1}, \quad (2.1)$$

in the Schwarzschild geometry of radial coordinate  $r$  and time  $t$  of an observer at infinity. The TOV equation is the equilibrium balance between the gravitational and radiation forces. Within the  $r$ -sphere, the total energy mass  $m(r) = M + E_\gamma(r) \approx M$  and the photon-pair fluid energy  $E_\gamma(r)$  is much smaller than the black hole mass  $M$ .

Rescaling the radius  $r$  in the unit of  $2GM$  and density  $\rho_\gamma$  in the unit of  $\rho_M = M/V_M$ , where “volume”  $V_M = (4\pi/3)(2GM)^3$ , we recast the TOV equation (2.1) as a

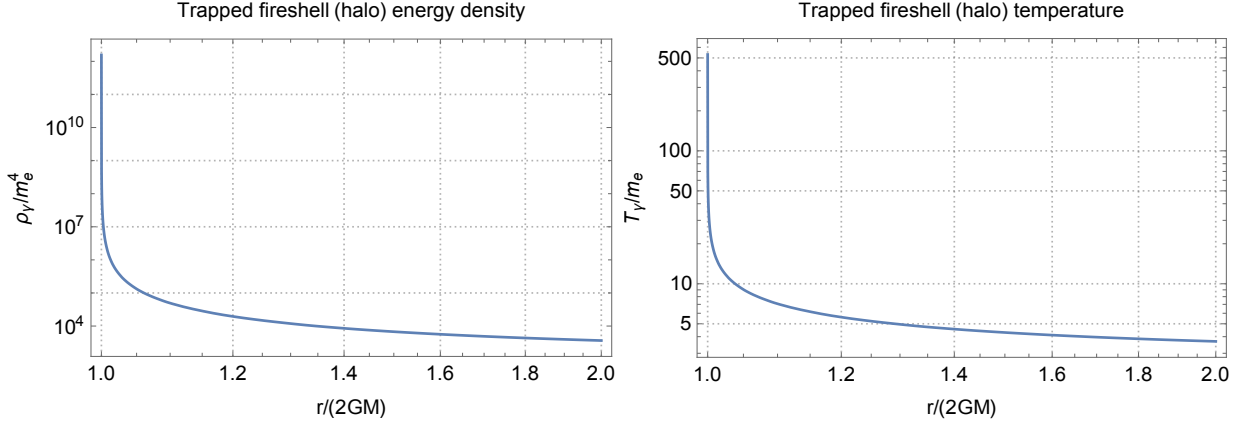


**Figure 2.** Left: the trapped fireshell (halo) energy density  $\rho_\gamma$  is expressed in units of  $m_e^4$  and as functions of radius  $r$ , which is in the unit of the horizon radius  $r_+ = 2GM = 2.33 \times 10^6$  cm for the black hole mass  $M = 7.75M_\odot$  (2.3). Right: the trapped fireshell (halo) temperature  $T_\gamma$  is expressed in units of the electron mass  $m_e \approx 0.5\text{MeV}$ . The maximal temperature  $T_\gamma^+$  near the horizon rapidly decreases to the asymptotic value  $\approx 2m_e$  near the boundary  $2r_+ = 4GM$ , where the electron-positron pair annihilation takes place. The Compton energy density  $m_e^4 \approx 4.54 \times 10^{21}\text{erg/cm}^3$  is of the same order as the critical energy density  $\rho_c = E_c^2/(8\pi) = 5.45m_e^4$ , where  $E_c = m_e^2/e$  is the critical electric field for electron and positron pair production in the semi-classical approximation [19]. We use the  $\hbar = c = 1$  and Compton unit of the electron mass  $m_e$ , unless otherwise specified.

dimensionless equation

$$\frac{d}{dr} \left( \frac{\rho_\gamma}{\rho_M} \right) = -\frac{3}{2r^2} \left( \frac{\rho_\gamma}{\rho_M} \right) \left[ 1 + r^3 \left( \frac{\rho_\gamma}{\rho_M} \right) \right] \left( 1 - \frac{1}{r} \right)^{-1}, \quad (2.2)$$

for the density  $\rho_\gamma$ . The photons and pairs flux  $F_\gamma = \rho_\gamma c$  and luminosity  $L_\gamma = 4\pi r^2 \rho_\gamma c$ .

The “density”  $\rho_M = M/V_M$  varies from  $(2 - 10)\rho_n$  for the mass  $M$  varies from  $(3 - 10)M_\odot$ . Here, we consider a massive stellar baryon core of neutron stars at the nuclear density  $\rho_n$ , gravitationally collapsing to a compact object of size about  $2GM$  of the black hole horizon. The average baryon density increases and becomes about  $5 \sim 8$  times the nuclear energy density. We choose (i)  $\rho_M = 10\rho_n$  that effectively corresponds to a black hole of the mass  $M$  and horizon radius  $r_+$

$$M = 7.75M_\odot, \quad r_+ = 2GM = 2.33 \times 10^6 \text{cm}; \quad (2.3)$$

(ii) the photon and pair density and luminosity near the horizon are

$$\rho_\gamma^+ \equiv \rho_\gamma(r_+) = \eta\rho_M = \rho_n, \quad L_\gamma^+ \equiv L_\gamma(r_+) = \eta L_{\text{pl}}, \quad (2.4)$$

$\eta = 0.1$  and the “Planck luminosity”  $L_{\text{pl}} \equiv 4\pi r_+^2 \rho_M c = (3/2)m_{\text{pl}}^2 = 3.73 \times 10^{59}\text{ergs/sec}$ . These are the boundary conditions for the ordinary differential equation (2.2). We chose  $\rho_\gamma^+ = \rho_n$  for the reason that at high temperatures, many species of relativistic particles, lepton-antilepton pairs and photons, light quark-antiquark pairs and gluons,

can be excited, contributing to the energy density  $\rho_\gamma^+$ . It is a fluid of lepton-photon and quark-gluon plasma. The essential quantity is the averaged energy over species  $d_f$ , i.e., the fluid temperature  $T_\gamma(r)$  (2.8) and value  $T_\gamma^+$  (2.9) near the horizon.

Solving the TOV equation (2.2) with boundary conditions (2.4), we show on the left (right) of Figs. 2 that the energy density  $\rho_\gamma$  (the temperature  $T_\gamma$ ) of photons and pairs is maximal near the horizon  $r_+$  and rapidly decreases as the radius increases to  $2r_+$ . The “trapped fireshell (halo)” is named for such an energetic fluid configuration of photons and pairs near the black hole horizon, where the maximal gravity effect confines the opaque fluid of photons and pairs. The macroscopic time scale of hydrodynamical relaxation for establishing a trapped fireshell is about  $\bar{R}/v_s$ , where the fluid sound velocity  $v_s = (P_\gamma/\rho_\gamma)^{1/2} = c/\sqrt{3}$ .

The total trapped fireshell energy is an integration over the energy density  $\rho_\gamma$  from the horizon  $r_+ = 2GM$  up to the boundary  $\bar{R} = 4GM = 2r_+$

$$E_\gamma(r) = \int_{r_+}^{2r_+} \rho_\gamma(r) \frac{4\pi r^2 dr}{(1 - \frac{r_+}{r})^{1/2}} = \rho_\gamma^+ 4\pi r_+^2 \delta\ell, \quad (2.5)$$

which is the energy of photons and pairs, as will be discussed below. Since the energy density  $\rho_\gamma(r)$  of photons and pairs is highly peaked near the horizon, as shown in Figs. 2, we use the  $\delta$ -function approximation  $\int (1 - r_+/r)^{-1/2} \rho_\gamma(r) dr \approx \rho_\gamma(r_+) \delta\ell$ , and  $\delta\ell = (1 - r_+/r)^{-1/2} dr$  is a proper distance near the horizon. The macroscopic length  $\delta\ell$  should be much larger than the Compton length  $\lambda_e$ , but smaller than the halo size  $2GM \approx 2.33 \times 10^6 \text{cm}$ . The total halo energy  $E_\gamma$  must be less than the maximal gravitational binding energy  $GM^2/(2r)|_{r=2GM} = M/4$ , which can be gained in collapses.

## 2.2 Thermodynamic and opaque fluid of photons and pairs

In the local Lorentz frame, we discuss thermodynamic quantities, e.g., temperature  $T_\gamma$ , of the opaque fluid of photons and pairs. The photons and electron-positron pairs’ energy (number) density  $\rho_\gamma$  ( $n_\gamma$ ) is extremely large inside the trapped fireshell. The mean free path  $\xi_\gamma = (\sigma_\gamma n_\gamma)^{-1}$  and the thermalization time scale  $\tau_\gamma = (\sigma_\gamma n_\gamma)^{-1} c$  are much smaller than the macroscopic size  $\bar{R}$  and the time scale  $\bar{R}/v_s$ . Therefore, the local thermal equilibrium is almost instantly established via the back-and-forth process  $\gamma + \gamma \leftrightarrow e^+ + e^-$  of the cross section,

$$\sigma_\gamma \approx \sigma_T \frac{3}{8\omega_\gamma} [\ln(2\omega_\gamma) - 1], \quad \omega_\gamma = \frac{T_\gamma}{m_e} \gg 1, \quad (2.6)$$

and time and length scales are

$$\tau_\gamma = \xi_\gamma = (\sigma_\gamma n_\gamma)^{-1} \approx \left[ \sigma_T n_\gamma \frac{3}{8\omega_\gamma} [\ln(2\omega_\gamma) - 1] \right]^{-1}, \quad (2.7)$$

where the Thomson cross section  $\sigma_T = (8\pi/3)\alpha^2/m_e^2$  and the fine structure constant  $\alpha = 1/137$ .

The local temperature  $T_\gamma(r)$  represents the mean kinematic energy of photons and electron-positron pairs, which possess zero chemical potential. As a result, the trapped

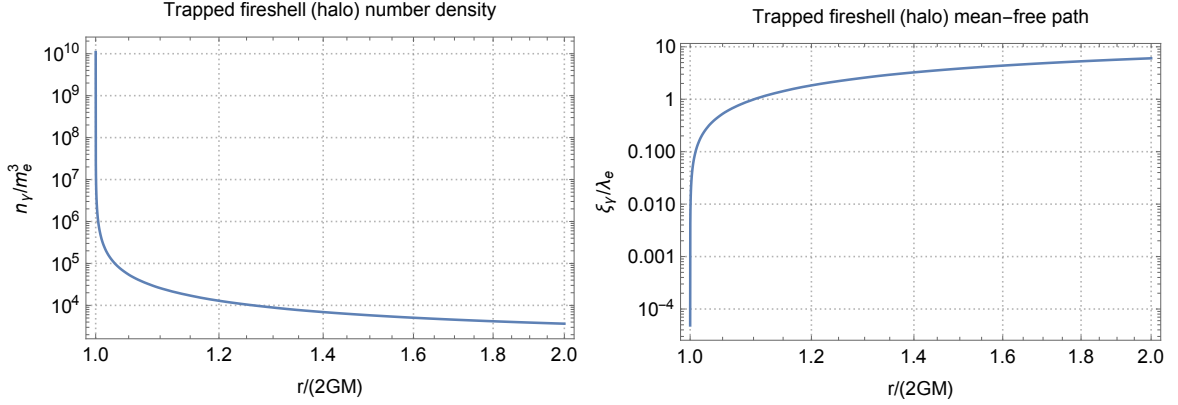


**Figure 3.** The photon and pair number density  $n_\gamma$  (left) and mean-free path  $\xi_\gamma = (\sigma_\gamma n_\gamma)^{-1}$  (right) are plotted as functions of radius  $r$  in the local observer frame. The Compton number density  $m_e^3 = 1.74 \times 10^{35}/\text{cm}^3$  and length  $\lambda_e = m_e^{-1} = 3.86 \times 10^{-11}\text{cm}$ .

fireshell is an electrically neutral, opaque and thermalised fluid of photons and electron-positron pairs. We describe it by a thermodynamic state of thermal temperature  $T_\gamma(r)$ , energy and number densities

$$\rho_\gamma(r) = \sigma_{\text{SB}} d_f T_\gamma^4(r), \quad n_\gamma(r) = \frac{30\zeta(3)}{\pi^4} d_f \sigma T_\gamma^3 = 3.7 d_f \sigma_{\text{SB}} T_\gamma^3(r), \quad (2.8)$$

in the local frame at the radius  $r$ . The Stefan-Boltzmann constant  $\sigma_{\text{SB}} = \pi^2/15$  for setting the Boltzmann constant  $k_B = 1$ . Here, we adopt  $d_f \approx 30$  for the number of massless gauge bosons and light fermion-antifermion pairs in the Standard Model (SM) of fundamental particle physics<sup>1</sup>, which can kinematically participate in the thermal equilibration at temperature  $T_\gamma > 10$  MeV. The boundary conditions (2.4) gives the horizon temperature  $T_\gamma^+$  near the horizon  $r_+ = 2GM$ ,

$$T_\gamma^+ \equiv T_\gamma(r_+) = \rho_\gamma^+ / (\sigma_{\text{SB}} d_f), \quad (2.9)$$

whose value depends on the balance between ultra-relativistic particles and gravitational pressures. In general, the horizon temperature represents the maximum temperature of trapped photon-pair spots at the place where the gravitational force is maximum. The horizon temperature  $T_\gamma^+ > 2m_e$  is a necessary condition, and  $T_\gamma^+ > 10$  MeV for the photon and pair energy density  $\rho_\gamma^+ \approx \rho_n$  is about the nuclear density. We use the electron-positron pair ( $e^-e^+$ ) notion for all possible SM pairs, and use the subscript “ $\gamma$ ” for the quantities of the trapped fireshell of photons and pairs.

As shown in Figs. 2 and 3, the trapped fireshell’s energy, number densities, and temperature are maximal near the horizon and decrease rapidly in radius. It forms a spherical incandescent halo of ultra-relativistic photons and pairs near the horizon. The halo width is about  $2GM = 1.16 \times 10^6$  cm for the temperature varying from the maximum  $\sim 10^2$  MeV near the horizon to  $\sim 1$  MeV near the outer boundary. The halo

<sup>1</sup>Since the number density is so high, see Fig. 3, neutrinos and anti-neutrinos can be possibly kept inside the fluid in participation of thermalisation.

ends at the outer boundary, where electrons and positrons annihilate to two low-energy ( $< 1$  MeV) photons, and the reverse process is kinematically impossible. The total number of photons and pairs is enormous

$$N_\gamma = \int_{r_+}^{2r_+} n_\gamma(r) \frac{4\pi r^2 dr}{(1 - \frac{r_+}{r})^{1/2}} \approx n_\gamma^+ 4\pi r_+^2 \delta\ell, \quad (2.10)$$

and  $n_\gamma^+ \equiv n_\gamma(r_+)$ , corresponding to the total energy  $E_\gamma$  (2.5). Here, the macroscopic length  $\delta\ell$  is approximately equal to the one in Eq. (2.5) for the total energy. Therefore, we effectively describe the trapped fireshells by the temperature  $T_\gamma^+$  and length  $\delta\ell$ .

As shown in Fig. 3, the mean-free path (2.7) are small; photons and pairs are not free streaming outward, and the luminosity  $L_\gamma = 4\pi r^2 \rho_\gamma c$  represents the diffusion flux of photons and pairs inside the halo. In the microscopic scale around each local point  $r$  of the halo, random particle collisions in all directions, the thermal equilibrium state and temperature  $T_\gamma(r)$  are isotropic without any preferential direction. However, at the macroscopic scale, the temperature  $T_\gamma(r)$  gradient is large in the radial direction due to the strong gravitational field near the horizon.

We use the local temperature  $T_\gamma$  to quantitatively describe a macroscopic-sized halo of the opaque thermal fluid of energetic photons and pairs, which is trapped around spherical black hole horizons following massive core collapses. One can generalise such a halo to macroscopic-sized spots in strong gravity and non-spherically symmetric environments of astrophysical accretion and coalescence in the presence of angular momentum, magnetic fields and other components.

Such a temperature  $T_\gamma(r)$  gradient results in a radially outward diffusion flux of photons and pairs, dissipating the halo energy  $E_\gamma$  (2.5) to the blackbody radiation and the emissions of UHE particles, as speculated in Refs. [24, 25] and will be discussed below. Therefore, the halo should be a metastable configuration that gradually shrinks and disappears. However, compared with the halo hydrodynamical relaxation On a time scale  $2r_+/v_s$ , the rate of energy dissipation is low, so we approximate the halo as a steady-state configuration of thermal energy sources.

We now turn to discussions of the dynamics of accelerating UHE particles on microscopic scales  $\sim 10^{-2}$  cm. Such a dynamics depends only on the local temperature of the spots, independently of the macroscopic sizes and global symmetries of the fire spots.

### 3 Compton-rocket effect on accelerating electrons

#### 3.1 Optically thin plasma of electrons and protons irradiated by photons

Reference [5] studies the Compton-rocket effect: via Thomson scattering, the radially outward photon flux (intensity)  $F_\gamma(r) = \rho_\gamma(r)c$  acts as a radiation force on an optically thin gas of hot electrons or cold protons, and accelerates them to high energies. The photon-scattering excess force on an isotropic gas results from the globally anisotropic loss of internal radiation energy. The rates of energy and momentum transfer from the



radiation flux  $F_\gamma(r)$  to the electron gas are (per electron),

$$\frac{d\epsilon_e}{d\tau} = -\sigma_T F_\gamma(r) [(4/3)(\beta_e \gamma_e)^2], \quad (3.1)$$

$$\frac{dp_e}{d\tau} = \sigma_T F_\gamma(r) [(2/3)(\beta_e \gamma_e)^2 + 1], \quad (3.2)$$

with the accelerated electron velocity  $\beta_e = v_e/c$ , Lorentz factor  $\gamma_e = (1 - \beta_e^2)^{-1/2}$ ,  $(\beta_e \gamma_e)^2 = \gamma_e^2 - 1$  and momentum  $p_e = m_e \beta_e \gamma_e$ . Here, we use a local observer's proper time  $\tau$  in a flat Lorentz frame at the radius  $r$ . Moreover, to simplify the notations consistently with the following discussed one-dimensional model, we do not specify the averages over the electron distribution in the momentum phase space [5]. Equation (3.2) gives the Eddington luminosity argument for the incident radiation pressure on non-relativistic electrons ( $\beta_e \approx 0$ ) in the Thomson scattering limit. For the proton case, these formulae remain the same with the substitutions of the subscript  $e \rightarrow p$  and approximate cross section  $\sigma_T \rightarrow \sigma_T^p \approx (m_e/m_p)^2 \sigma_T \ll \sigma_T$  of multi-photons and proton collisions.

It is worthwhile to emphasise that the Compton-rocket effect (3.1, 3.2), where present the photon flux  $F_\gamma(r)$ , is essentially attributed to the nonlinear QED processes of multi-photon scatterings and interactions (see, e.g., [26–28]). These non-linear interactions are particularly important when the radiation field is energetic and the charged particle density is large. It is what we will study in the following sections.

### 3.2 Electrons and protons in an opaque fluid of photons and pairs

The trapped fireshell (halo) of photons and pairs around the black hole horizon has an ultra-high temperature  $T_\gamma$ , see Fig. 3. All material electrons and protons are ionised inside the fluid. Their average densities are much smaller than the density of photons and pairs. They have nonzero chemical potentials and do not participate in the thermal equilibrium of photons and pairs via the process  $\gamma + \gamma \leftrightarrow e^+ e^-$ . They couple with photons and pairs via multi-particle collisions and field interactions, and are in an energy equipartition with photons and pairs. Electrons are relativistic, protons are non-relativistic, and they do not form an electron-proton oscillating plasma. We describe them by the number of bulk electrons and protons inside the fluid,

$$\bar{N}_e = \bar{N}_p = B N_\gamma, \quad \gamma_e = \langle \tilde{\gamma}_e \rangle = 1, \quad \beta_e = \langle \tilde{\beta}_e \rangle = 0. \quad (3.3)$$

Here, the baryon-loading  $B \ll 1$  quantifies the total number of electrons (protons) inside an opaque spot of photons and pairs of the number  $N_\gamma$ . The  $B$  should relate to the baryon loading of fireballs, whose outward expansion accounts for GRBs. The  $\tilde{\gamma}_e$  and  $\tilde{\beta}_e$  represent the velocity and Lorentz factor of bulk electrons, randomly colliding with photons and pairs. The averages  $\langle \tilde{\beta}_e \rangle = 0$  and  $\langle \tilde{\gamma}_e \rangle = 1$  are over the distribution of bulk electrons.

In a one-dimensional model for the spherical symmetric fireshell, the bulk electrons averaged momentum  $\langle \tilde{p}_e \rangle = m_e \langle \tilde{\beta}_e \gamma_e \rangle$  vanishes with the random distribution  $\propto e^{-\tilde{p}_e^2/T_\gamma}$  with an equal probability of inward and outward moving. Thus, bulk electrons do

not have a net drift in the direction  $\hat{r} > 0$  or opposite one  $\hat{r} < 0$ , and their averaged velocity vanishes  $\langle \tilde{\beta}_e \rangle = 0$  and  $\langle \tilde{\gamma}_e \rangle = 1$ , and the same discussions for bulk protons  $\bar{N}_p$ .

However, the situation changes when the strong radiation force (3.2) is present, acting on bulk electrons, since the density of photons and pairs has a large variation gradient in the radial direction, as shown in Figs. 2 and 3. We attempt to investigate the Compton-rocket effect on bulk electrons in a highly opaque fluid of photons and pairs at high temperatures  $T_\gamma \gg m_e$ , densities  $\rho_\gamma \gg m_e^4$  and  $n_\gamma \gg m_e^3$ . Namely, how the radially outward flux (intensity)  $F_\gamma(r) = \rho_\gamma(r)c \gg m_e^4$  acts as a radiation force on bulk electrons and protons (3.3), accelerating them outward along the radial direction to high energies.

This system is more complex than an optically thin electron-proton plasma irradiated at energies  $\epsilon_\gamma \sim m_e$  photons, numerically studied, see e.g. Refs. [11, 29]. Nevertheless, to gain an insight into the dynamics of the Compton-rocket effect on bulk electrons and protons, we use a simplified one-dimensional model in the radial direction only. The photons and pairs flux  $F_\gamma = \rho_\gamma(r)c$  acts on bulk electrons in a tiny tube with the cross section  $\sigma_\gamma$ .

### 3.3 Drifting electrons in an opaque fluid of photons and pairs

Although the mean-field path of bulk electrons is small, as shown in Fig. 3, the outward radiation force  $F_\gamma = \rho_\gamma(r)c$  is strong, so some bulk electrons have chances within their mean-free path to get accelerated and drift radially outwards. Therefore, some bulk electrons drift in the direction  $\hat{r} > 0$  and their averaged momentum  $p_e = \langle \tilde{p}_e \rangle_a$  and energy  $\epsilon_e = (p_e^2 + m_e^2)^{1/2}$  do not vanish. We define the number density of these outward drifting electrons as

$$N_e(\gamma_e) < \bar{N}_e, \quad \beta_e = \langle \tilde{\beta}_e \rangle_a > 0, \quad \gamma_e = \langle \tilde{\gamma}_e \rangle_a > 1, \quad (3.4)$$

where the average  $\langle \cdot \cdot \rangle_a$  is over the distribution of bulk and drifting electrons. The drifting electrons should be a small fraction of the bulk electrons. The same discussions apply to drifting  $N_p$  and bulk  $\bar{N}_p$  protons in the opaque fluid of photons and pairs.

We further examine the time scale  $\tau_a^e$  of the electron acceleration process and compare it with the thermalisation time scale  $\tau_\gamma = (\sigma_\gamma n_\gamma)^{-1}c$  (2.7) of photon and pair fluid. Using Eq. (3.2) we define

$$\tau_a^e \equiv \frac{p_e}{dp_e/d\tau} = \frac{m_e \beta_e \gamma_e}{\sigma_T F_\gamma [\frac{2}{3}(\beta_e \gamma_e)^2 + 1]}, \quad (3.5)$$

and obtain the ratio

$$\frac{\tau_a^e}{\tau_\gamma} = \frac{3.7 \times 9}{16\omega_\gamma^2} \frac{\ln(2\omega_\gamma) - 1}{(\beta_e \gamma_e) \left[ 1 + \frac{3}{2(\beta_e \gamma_e)^2} \right]}. \quad (3.6)$$

where the gravitational time dilation factors  $d\tau = (1 - 1/r)^{1/2}dt$  are simplified. Recall that the thermalisation time scale  $\tau_\gamma$  (2.7) represents also the time scale of the flux  $F_\gamma$  of multi-photons acting on a changed particle.

The time and length scales  $\tau_a^e$  of the Compton-rocket effect are smaller than the thermalisation timescale  $\tau_\gamma$  of photons and pairs fluid, i.e.,  $\tau_a^e < \tau_\gamma$ , for  $\omega_\gamma = T_\gamma/m_e > 1$  and  $\gamma_e > 1$ . The drifting electron density  $n_e(\gamma_e)$  is much smaller than the density  $n_\gamma$  of photons and pairs. These properties imply that drifting electrons accelerated by the Compton-rocket effect are small and rapid perturbations upon the thermal bath of photons and pairs at high energies and densities. If the timescale inequality was  $\tau_a^e > \tau_\gamma$  instead of  $\tau_a^e < \tau_\gamma$ , the perturbations of drifting electrons would have been washed out by photon-pair thermal fluctuations. The drifting electron perturbation's energy and momentum are  $\delta\epsilon_e > m_e$  and  $\delta p_e > m_e$  with Lorentz factor  $\gamma_e \gtrsim 1$ .

Moreover, due to the large opacity and frequent collisions with photons and pairs, drifting electrons ( $\gamma_e \gtrsim 1$ ) quickly dissipate their energy and run back to bulk electrons ( $\gamma_e = 1$ ), which are in an energy equipartition with photons and pairs. It implies that the perturbations of drifting electrons ( $\gamma_e > 1$ ) should be rapidly washed out. Therefore, it looks unlikely that in the opaque fluid of photons and pairs, such small perturbations could develop, namely, accelerated electrons by the Compton-rocket effect could drift to a large Lorentz factor  $\gamma_e \gg 1$ , unless some instabilities of avalanche phenomena occur.

## 4 Runaway electrons in an opaque fluid photons and pairs

### 4.1 Accelerated electron runaway due to Klein–Nishina corrections

As discussed, in the opaque fluid of photons and pairs, the Compton-rocket effect on accelerating electrons is an approximately “local” and “instantaneous” perturbation that triggers electrons to increase energy and drift in the outward radial direction. On their way, accelerated electrons collide with photons and pairs with the probability described by the Klein–Nishina (KN) cross section (4.1), which, however, decreases as the accelerated electrons' energy increases, and the straightforward scattering with a narrower deflection angle  $\theta_e \sim 0$ . This property of KN corrections implies the instability of an unstable avalanche runaway process. Namely, accelerated electrons gain more energy and have fewer collisions. Thus, they have greater chances to drift a longer distance and gain even more energy from the Compton-rocket effect. As a result, there is a probability that a small fraction of drifting electrons run away and achieve ultra-high energies, penetrating through the opaque fluid of photons and pairs.

In the opaque fluid of photons and pairs at the temperature  $T_\gamma > m_e$ , drifting electrons move outward in the radial direction  $\theta_e \sim 0$ , with the velocity  $\beta_e \sim 1$  and Lorentz factor  $\gamma_e > 1$ . The KN cross-section is approximately given by

$$\sigma_{\text{KN}}^e \approx \sigma_T \frac{3}{8\omega_e} \left[ \ln(2\omega_e) + \frac{1}{2} \right], \quad \omega_e \approx \frac{2T_\gamma}{m_e} \gamma_e, \quad (4.1)$$

where the factor 2 in  $\omega_e$  (4.1) is due to the blue-shift effect [30]. The cross-section decreases as the drifting electrons' Lorentz factor  $\gamma_e$  increases and vanishes when  $\gamma_e \gg 1$ . Therefore, high  $\gamma_e$  drifting electrons have a small probability of being scattered back to bulk electrons with  $\gamma_e = 1$ . Instead, they are further accelerated to higher  $\gamma_e$  by the Compton-rocket effect, and behave as runaway electrons.

Such a runaway process has a time scale  $\tau_{\text{KN}}^e = (\sigma_{\text{KN}}^e n_\gamma c)^{-1}$  of the instability, which is much larger than the thermalization time scale  $\tau_\gamma$  (2.7) of photons and pairs,

$$\frac{\tau_{\text{KN}}^e}{\tau_\gamma} \approx 2\gamma_e \frac{\ln(2T_\gamma/m_e)}{\ln(4\gamma_e T_\gamma/m_e)} \gg 1, \quad \gamma_e \gg 1, \quad (4.2)$$

and the gravitational time dilation factors  $d\tau = (1 - 1/r)^{1/2} dt$  are simplified. The time scales (3.5), (3.6) and (4.2) give  $\tau_a^e < \tau_\gamma \ll \tau_{\text{KN}}^e$ , implying that rather than being smeared out, the instability could develop a runaway solution. It makes drifting electrons start from microscopic perturbations (3.6) run to macroscopic motions (4.2). It is necessary to perform numerical simulations to verify that such an instability and runaway solution indeed occur in an opaque fluid of photons and pairs at high temperature  $T_\gamma \gg m_e$ .

## 4.2 Electrons accelerated by photons and pairs at high temperature

Even if this instability occurs, what is the significant probability of runaway drifting electrons that survive over a long macroscopic distance and time scale, reaching ultra-high energies? We describe this probability by the fraction  $N_e(\gamma_e)/\bar{N}_e$  of drifting and bulk electrons. To study this fraction, we rewrite the Compton-rocket effect on the electron acceleration (3.2) in a small distance  $dr = \beta_e d\tau = \beta_e(1 - r_+/r)^{1/2} dt$  as

$$m_e^{\text{eff}} \gamma_e \frac{d\gamma_e}{dr} = \frac{1}{3} \sigma_T (1 - r_+/r)^{-1/2} F_\gamma(r) (2\gamma_e^2 + 1). \quad (4.3)$$

In the one-dimensional model, this equation represents drifting electrons  $N_e(\gamma_e)$  of  $\gamma_a > 1$  accelerated out from bulk electrons  $\bar{N}_e$  of  $\gamma_e = \langle \tilde{\gamma}_e \rangle = 1$ . The effective mass  $m_e^{\text{eff}} \approx m_n + m_e$  will be explained in due course.

First, we consider an unrealistic situation where all bulk electrons  $\bar{N}_e$  (3.3) are accelerated to drifting electrons  $N_e(\gamma_e)$  in the radial direction without any collision with photons and pairs. Then integrating the Compton-rocket effect (4.3) yields

$$2\gamma_e^2 + 1 = 3 \exp \left[ \frac{4\sigma_T}{3m_e^{\text{eff}}} \int_{r_+}^r \frac{\rho_\gamma(r')}{(1 - r_+/r')^{1/2}} dr' \right], \quad (4.4)$$

where bulk electrons  $\gamma_e = 1$  near the horizon  $r_+$  are accelerated to drifting electrons  $\gamma_e > 1$  at the radius  $r$ . The photon and pair flux  $F_\gamma(r) = \rho_\gamma c$  is highly peaked and has a great gradient near the horizon  $r_+$ , as shown in Fig. 2. Therefore, the photon and pair flux  $F_\gamma(r_+) = \rho_\gamma(r_+)c$  and temperature  $T_\gamma(r_+)$  (2.9) near the horizon predominantly contribute to the integration (4.4), i.e., to the acceleration of drifting electrons out from bulk electrons. Similarly to Eq. (2.5) for the total energy, we use the  $\delta$ -function approximation  $\int (1 - r_+/r)^{-1/2} \rho_\gamma(r) dr \approx \rho_\gamma(r_+) \delta\ell = \sigma_{\text{SB}} d_f T_\gamma^4(r_+) \delta\ell$ , where  $\delta\ell = (1 - r_+/r)^{-1/2} dr$  is a small proper distance near the horizon. Solution (4.4) approximately becomes

$$2\gamma_e^2 + 1 \approx 3 \exp \left[ \frac{4\sigma_T \sigma_{\text{SB}} d_f}{3m_e^{\text{eff}} m_e} T_\gamma^4(r_+) \delta\ell \right], \quad (4.5)$$

namely, the radiation force  $F_\gamma(r_+) = \rho_\gamma(r_+)c$  accelerates an electron over a distance  $\delta\ell$  to reach its Lorentz factor  $\gamma_e$ .

In the viewpoint of the energy density  $\rho_\gamma \sim T_\gamma^4 \sim E_{\text{eff}}^2/(8\pi)$ , the photons and pairs radiation force (pressure)  $F_\gamma = c\rho_\gamma$  for the temperature  $T_\gamma^+ \equiv T_\gamma(r_+) \sim \mathcal{O}(10^{1-2})\text{MeV}$  is equivalent to an effective electric force  $eE_{\text{eff}}$ , which is about  $\mathcal{O}(10^{1-2})$  times larger than the critical electric field force  $eE_c = m_e^2$  for electron-positron pair productions. In a classical scenario for a test charged particle accelerated by an electric field, we estimated that such an effective electric force  $eE_{\text{eff}}$  accelerates an electron to  $\text{PeV} \sim 10^9 m_e(\gamma_e \sim 10^9)$  energies in a small distance  $d \sim \mathcal{O}(10^9)\lambda_e \sim \mathcal{O}(10^{-2})\text{ cm}$  and time  $\tau = d/c \sim \mathcal{O}(10^{-12})\text{ sec}$  [24]. Therefore, the macroscopic length  $\delta\ell$  determined from the total thermal energy  $E_\gamma$  (2.10) should be large enough for an electron reaching  $\gamma_e \sim 10^9$  in Eq. (4.5). It indicates that the macroscopic sizes and geometries of dense and energetic photon and pair spots are irrelevant for the Compton-rocket effect, because the local inhomogeneous density of photons and pairs accelerates electrons on microscopic time and length scales.

Physically, the solution (4.5) without any collision means that (i) all bulk electrons  $\bar{N}_e$  of  $\gamma_e = 1$  accelerated to drifting electrons  $N_e(\gamma_e)$  of an enormous Lorentz factor  $\gamma_e \gg 1$ ; (ii) the majority of drifting electrons get accelerated and reach their ultra-high energies in the neighbourhood near the horizon. This collisionless solution (4.5) of  $N_e(\gamma_e) = \bar{N}_e$  is certainly not realistic, since the fluid of photons and pairs is extremely opaque.

### 4.3 Superthermal spectrum of UHE electrons

#### 4.3.1 Thomason scattering in low energies

Second, we consider the case of the constant Thomason cross section  $\sigma_T$  in low energies (temperatures). We calculate the number of drifting electrons accelerated in one proper mean-free path  $\xi_e^T = (n_\gamma\sigma_T)^{-1}$  and time  $d\tau = \xi_e^T/\beta_e$ . The acceleration equation (3.2) for the Lorentz factor variation  $\Delta\gamma_e$  in one mean-free path becomes

$$m_e^{\text{eff}}\gamma_e\Delta\gamma_e^T = \frac{1}{3}\sigma_T F_\gamma(r)(2\gamma_e^2 + 1)\xi_e^T. \quad (4.6)$$

Using the relation  $F_\gamma/n_\gamma = T_\gamma/3.7$ , the variation  $\Delta\gamma_e^T$  in one mean-free path is given by

$$\Delta\gamma_e^T = \frac{1}{3.7} \left( \frac{T_\gamma}{m_e^{\text{eff}}} \right) \frac{2\gamma_e^2 + 1}{3\gamma_e}, \quad (4.7)$$

which is proportional to  $(T_\gamma/m_e^{\text{eff}})\gamma_e$  for  $\gamma_e \gg 1$ .

Due to the Thomson scatterings with photons and pairs, the drifting electron numbers  $N_e(\gamma_e)$  decrease following the one-dimensional rate equation,

$$\frac{dN_e}{dr} = -\frac{1}{\xi_e^T}N_e = -n_\gamma\sigma_T N_e, \quad (4.8)$$

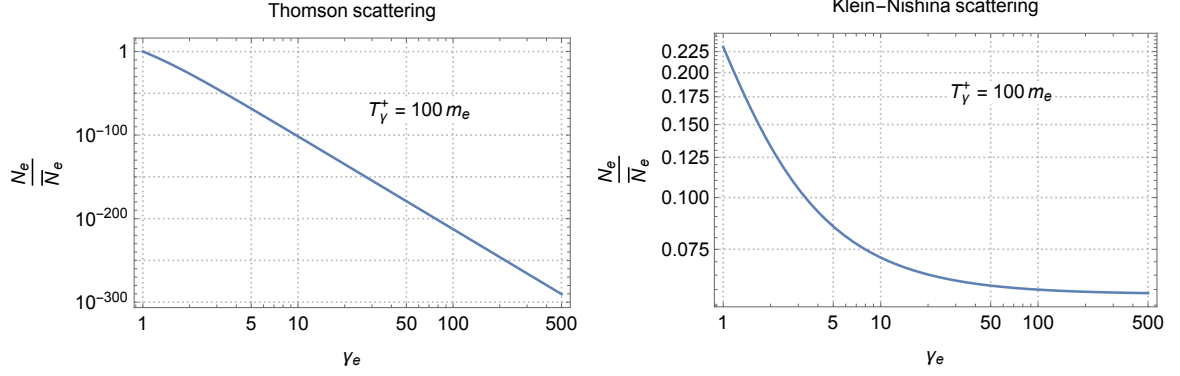


**Figure 4.** We calculate the fraction  $N_e/\bar{N}_e$  of accelerated electrons drifting out of the bulk electrons for the Thomson (4.10) and the Klein-Nishina (4.15) scattering cases. It shows that the probability of accelerated electrons reaching high energies is non-trivial, implying the runaway behaviour, in the Klein-Nishina scattering case, but is completely negligible in the Thomson scattering case. These figures also present the proton case with the substitution of the subscript  $e \rightarrow p$ .

similarly to the equation for unstable particles of the number  $N_e$  decaying while travelling along the radial trajectory. The rate equation (4.8) recasts as

$$\frac{dN_e(\gamma_e)}{d\gamma_e} = -\frac{1}{\Delta\gamma_e^T} N_e(\gamma_e), \quad (4.9)$$

by using Eqs. (4.3) and (4.6).

Assuming that the majority of drifting electrons get accelerated in the neighbourhood near the horizon, as discussed in Eq. (4.5), we approximate the temperature  $T_\gamma \approx T_\gamma^+$  by the horizon temperature  $T_\gamma^+$ . Integrating the rate equation (4.9) shows the fraction (probability) of drifting electrons  $N_e(\gamma_e)$  out of bulk electrons  $\bar{N}_e$  ( $\gamma_e = 1$ ) is given by

$$\frac{N_e(\gamma_e)}{\bar{N}_e} = \exp - \int_1^{\gamma_e} \frac{1}{\Delta\gamma_e^T} d\gamma_e \approx \left( \frac{3}{2\gamma_e^2 + 1} \right)^{2.78(m_e^{\text{eff}}/T_\gamma^+)}. \quad (4.10)$$

As shown on the left of Fig. 4, the fraction  $N_e(\gamma_e)/\bar{N}_e$  decreases rapidly as the accelerated electron Lorentz factor  $\gamma_e$  increases on the way they travel outward, dissipating their energy and momentum into the fluid via collisions with photons and pairs due to the large opacity.

Thus, the most accelerated drifting electrons  $N_e(\gamma_e)$  at high energies run back to the bulk electrons  $\bar{N}_e$  at low energies, which are in the energy equipartition with photons and pairs. In other words, the probability of drifting electrons reaching a large Lorentz factor  $\gamma_e \gg 1$  goes to zero. Very few electrons are in the high-energy superthermal spectrum tail. It is the case for the Sun, whose core temperature of photons is much smaller than the electron mass, i.e.,  $T_\odot \approx 1.5 \times 10^4 \text{eV} \ll m_e$ .

### 4.3.2 Klein-Nishina scattering in high energies

Finally, we consider drifting electrons accelerated in one proper mean-free path  $\xi_e^{\text{KN}} = (n_\gamma \sigma_{\text{KN}}^e)^{-1}$ , and show they run away due to the energy-dependent Klein-Nishina cross section  $\sigma_{\text{KN}}^e(\gamma_e)$  (4.1). The acceleration equation (3.2) for the Lorentz factor variation  $\Delta\gamma_e^{\text{KN}}$  in one mean-free path becomes

$$m_e^{\text{eff}} \gamma_e \Delta\gamma_e^{\text{KN}} = \frac{1}{3} \sigma_T F_\gamma(r) (2\gamma_e^2 + 1) \xi_e^{\text{KN}}. \quad (4.11)$$

Using the relation  $F_\gamma/n_\gamma = T_\gamma/3.7$  and the KN cross section (4.1) that depends on drifting electrons'  $\gamma_e$ , the variation  $\Delta\gamma_e^{\text{KN}}$  in one mean-free path is given by

$$\Delta\gamma_e^{\text{KN}}(T_\gamma, \gamma_e) = \frac{1}{3.7} \frac{16}{9} \left( \frac{T_\gamma^2}{m_e m_e^{\text{eff}}} \right) \frac{2\gamma_e^2 + 1}{\ln(4\gamma_e \frac{T_\gamma}{m_e}) + \frac{1}{2}}, \quad (4.12)$$

in the contrast with Eq. (4.7) for the Thomason scattering case.

Analogously to Eqs. (4.8) and (4.9) in the Thomson scattering case, due to the Klein-Nishina scatterings with photons and pairs, the drifting electron number  $N_e(\gamma_e)$  decreases following the one-dimensional rate equation

$$\frac{dN_e}{dr} = -\frac{1}{\xi_e^{\text{KN}}} N_e = -n_\gamma \sigma_{\text{KN}}^e N_e, \quad (4.13)$$

which recasts as

$$\frac{dN_e(T_\gamma, \gamma_e)}{d\gamma_e} = -\frac{1}{\Delta\gamma_e^{\text{KN}}(T_\gamma, \gamma_e)} N_e(T_\gamma, \gamma_e), \quad (4.14)$$

by using Eqs. (4.3) and (4.11).

The integration of the rate equation (4.14) leads to the fraction (probability) of drifting electrons  $N_e(T_\gamma, \gamma_e > 1)$  out of bulk electrons  $\bar{N}_e(T_\gamma, \gamma_e = 1)$ ,

$$\frac{N_e}{\bar{N}_e} \equiv \frac{N_e(T_\gamma, \gamma_e > 1)}{\bar{N}_e(T_\gamma, \gamma_e = 1)} \approx \exp - \int_1^{\gamma_e} \frac{1}{\Delta\gamma_e^{\text{KN}}(T_\gamma^+, \gamma_e')} d\gamma_e'. \quad (4.15)$$

Here we approximate  $T_\gamma$  by the characteristic temperature  $T_\gamma^+$  for the same argument discussed in Eqs. (4.5) and (4.10). Figure 5 gives the numerical integration (4.15) that shows the non-trivial number of drifting electrons at ultra-high energies, which is in distinct contrast with the completely negligible one in the Thomason scattering case (4.10). This non-trivial number  $N_e$  of drifting electrons ( $\gamma_e \gg 1$ ) means a superthermal spectrum in the high-energy tail.

Figure 5 shows that for Lorentz factors  $\gamma_e < 10^3$ , (a) the accelerated electron fraction  $N_e/\bar{N}_e$  decreases as  $\gamma_e$  increases, which may approximate as a decay power law  $(\gamma_e)^{-\nu}$  ( $\nu > 0$ ); (b) the fraction approach a constancy  $(\gamma_e)^0$  for  $\gamma_e > 10^3$ :

$$(a) \frac{N_e}{\bar{N}_e} \propto (\gamma_e)^{-\nu}, \quad (\gamma_e < 10^3); \quad (b) \frac{N_e}{\bar{N}_e} \propto (\gamma_e)^0, \quad (\gamma_e > 10^3). \quad (4.16)$$



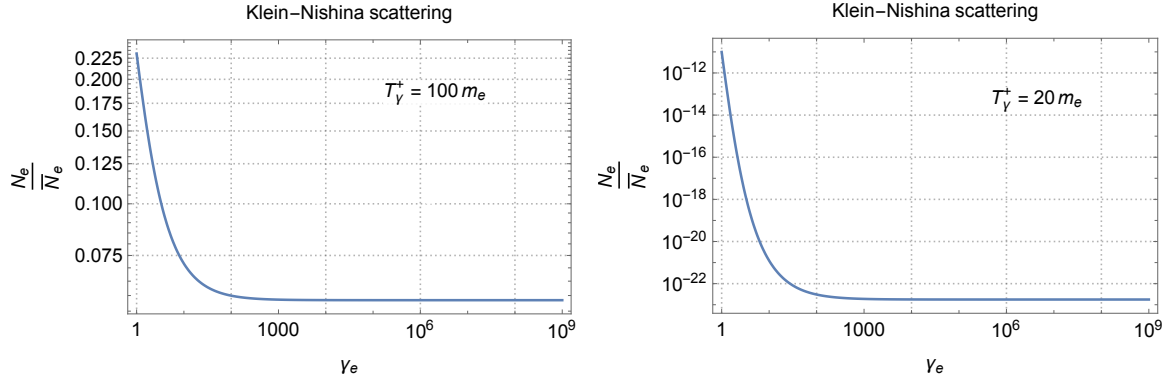


**Figure 5.** We show the fraction  $N_e/\bar{N}_e$  (4.15) of accelerated electrons drifting out of bulk electrons at different temperatures  $T_\gamma^+ \gg m_e$  near the horizon. The  $N_e/\bar{N}_e$  value is exponentially sensitive to the horizon temperature  $T_\gamma^+$ . The probability of accelerated electrons reaching high energies is small for temperatures  $T_\gamma^+ \lesssim 10m_e$ , and the Compton-rocket effect and runaway dynamics might not be observationally relevant. These figures also present the proton case by substituting the subscript  $e \rightarrow p$ .

The feature (a) is not unexpected in a usual physical situation where the probability of drifting electrons running to high energies becomes smaller. However, the feature (b) is peculiar, showing the high-energy superthermal spectrum tail becomes very flat when  $\gamma_e > 10^3$ . It is the exact attributes of unstable runaway behaviour. Since the KN cross-section decreases as the drifting electrons' energies increase, they continue accelerating to higher and higher energies by the Compton-rocket effect without dissipating much energy into photons and pairs. Such an avalanche dynamics is crucially important for producing UHE particles of Lorentz factors  $\gamma_e \gg 1$ .

Using  $\Delta\gamma_e^{\text{KN}}$  (4.12) and  $(N_e/\bar{N}_e)$  (4.15), we approximately calculate the asymptotic constancy for large  $\gamma_e > 10^3$

$$\left(\frac{N_e}{\bar{N}_e}\right)_{\gamma_e \gg 1} \approx \left(\frac{4T_\gamma^+}{m_e}\right)^\chi e^{-\chi}, \quad \chi = \frac{m_p}{m_e} \left(\frac{m_e}{T_\gamma^+}\right)^2, \quad (4.17)$$

which is exponentially suppressed by small horizon temperatures  $T_\gamma^+/m_e$ , as can be seen in Figs. 4 and 5. The excess of large  $\gamma_e$  electrons  $N_e$  in the superthermal tail deviating from the blackbody radiation spectrum in the case of the Sun ( $T_\odot/m_e \ll 1$ ) is too small to be relevant for observations. However, the probability of  $\gamma_e \gg 1$  electrons' excess may be relevant for the detections by laser experiments for the physics of strong radiation fields in future.

For the case of electron-proton plasma interacting with high-energy photons  $\epsilon_\gamma \sim m_e$ , Equations of types (4.8,4.9) or (4.13,4.14) were used in the numerical studies Ref. [11] to discuss the superthermal spectrum tail of runaway electrons  $N_e$  drifting backwards to massive protons due to the electric field induced by the charge separation between electrons and protons. Instead, we are in a situation where fully ionised electrons and protons are free, not in electron-proton plasma oscillations. They interact



with photons and pairs at very high temperatures  $T_\gamma \gg m_e$ , energy density  $\rho_\gamma \gg m_e^4$  and number density  $n_\gamma \gg m_e^3$ .

#### 4.4 Runaway protons pulled by runaway electrons

A non-trivial amount of high-energy electrons running away indicates that we cannot ignore protons in the Compton-rocket effect on electrons, because of the electric field  $E$  developed between separated electrons and protons. It is due to the very different cross sections  $\sigma_T \gg \sigma_T^p \approx (m_e/m_p)^2 \sigma_T$  of photons scattering with electrons and protons. The Compton-rocket effect on protons ( $p_p = m_p \beta_p \gamma_p$ )

$$\frac{d\epsilon_p}{d\tau} = -\sigma_T^p F_\gamma(r) [(4/3)(\beta_p \gamma_p)^2], \quad (4.18)$$

$$\frac{dp_p}{d\tau} = \sigma_T^p F_\gamma(r) [(2/3)(\beta_p \gamma_p)^2 + 1], \quad (4.19)$$

is much smaller than the one (3.2) on electrons.

As a result, charge separation and the electric field  $E_{pe}$  between electrons and protons occur. It must back-react on the one-dimensional acceleration equations for both electrons (3.2) and protons (4.19),

$$\frac{dp_e}{d\tau} = \sigma_T F_\gamma(r) [(2/3)(\beta_e \gamma_e)^2 + 1] - eE_{pe} > 0, \quad (4.20)$$

$$\frac{dp_p}{d\tau} = \sigma_T^p F_\gamma(r) [(2/3)(\beta_p \gamma_p)^2 + 1] + eE_{pe} \approx eE_{pe} > 0. \quad (4.21)$$

It is a highly non-linear dynamical system. We are interested in the situation when photons and pairs' radiation force  $\sigma_T F_\gamma \propto T_\gamma^4 (\beta_e \gamma_e)^2$  in Eq. (4.20) is so strong to accelerate a significantly non-trivial fraction  $N_e/\bar{N}_e$  of electrons drifting outward  $dp_e/d\tau > 0$  (4.20), and induce an electric field  $E_{pe} = eN_e/(4\pi r^2)$  to pull massive protons  $dp_p/d\tau \approx E_{pe} > 0$  (4.21) accelerating outwards in the radial direction, following the accelerated electrons. We assume that such a dynamical configuration can be realised by a large temperature  $T_\gamma \gg m_e$ , a significantly non-trivial fraction  $N_e/\bar{N}_e$  and a large Lorentz factor  $\gamma_e$ . It is necessary to verify it using numerical simulations, under what conditions to realise such a dynamical configuration. Since protons are massive, if the photons and pairs temperature  $T_\gamma$  is not large enough, instead of accelerating protons, the bulk electrons  $\bar{N}_e$  are accelerated backwards by the induced electric field  $E_{pe}$ , as numerically studied in Ref. [11].

In this speculated configuration, we set that the bulk and drifting electron numbers are identical to the bulk and drifting proton numbers

$$\bar{N}_e = \bar{N}_p, \quad N_e = N_p, \quad N_e/\bar{N}_e = N_p/\bar{N}_p, \quad (4.22)$$

because of the global charge neutrality and conservation. The combination of Eqs. (4.20) and (4.21) yields the acceleration equation for electrons and protons together

$$\frac{d(p_e + p_p)}{d\tau} \approx \sigma_T F_\gamma(r) [(2/3)(\beta_e \gamma_e)^2 + 1], \quad (4.23)$$

neglecting the radiation force on protons. Under the condition of a strong enough radiation flux  $F_\gamma$  and the electric field  $E$ , we further model that drifting electrons  $N_e$  and protons  $N_p$  are moving together

$$\beta_e \approx \beta_p \quad \text{and} \quad \gamma_e \approx \gamma_p, \quad (4.24)$$

through the fluid of photons and pairs. The acceleration equation (4.23) is simplified as

$$(m_e + m_p) \frac{d(\beta_e \gamma_e)}{d\tau} \approx \sigma_T F_\gamma(r) [(2/3)(\beta_e \gamma_e)^2 + 1], \quad (4.25)$$

which is the same as the electron acceleration equation (3.2) or (4.3) by introducing an effective electron mass  $m_e^{\text{eff}} = m_p + m_e \approx m_p$ . Similarly, the combination of (3.1) and (4.18) yields the energy-gain equation for accelerated electrons and protons

$$\frac{d\epsilon_{ep}}{d\tau} \approx -\sigma_T F_\gamma(r) [(4/3)(\beta_e \gamma_e)^2], \quad \epsilon_{ep} = \epsilon_e + \epsilon_p, \quad (4.26)$$

where  $\epsilon_e = m_e \gamma_e$  and  $\epsilon_p = m_p \gamma_p$ .

In the one-dimensional model, Equations (4.25) and (4.26) qualitatively describe an accelerating system of electrons and protons driven by the radiation force, assuming electrons and protons associated by their own electric field and accelerated to the approximately same Lorentz factor  $\gamma_e \approx \gamma_p$ . In this approximation, all dynamical equations remain the same, except for replacing the electron mass  $m_e$  with the effective electron mass  $m_e^{\text{eff}} = m_p + m_e$  for a heavy system of electrons and protons. As previously anticipated, the effective mass  $m_e^{\text{eff}} \gg m_e$  replaces  $m_e$  in the dynamic equations (4.3) and (4.25). As a consequence, the large temperature  $T_\gamma$  radiation flux  $F_\gamma$  acting on an electron is required to accelerate a heavy system of both electrons and protons.

In addition, when electrons and protons drift through the fluid of photons and pairs, they undergo Klein-Nishina scattering processes. The KN cross section  $\sigma_{\text{KN}}^p$  of drifting protons is much smaller than the one  $\sigma_{\text{KN}}^e$  (4.1) of drifting electrons, i.e.,  $\sigma_{\text{KN}}^p \sim \mathcal{O}[(m_p/m_e)^2] \sigma_{\text{KN}}^e$ . Therefore, we neglect the cross section  $\sigma_{\text{KN}}^p$  of drifting protons. In these approximations, all analyses and results in the previous sections remain the same. Both drifting electrons and protons run away, becoming UHE particles. Figures 5 also represent the fraction of accelerated protons with the substitution  $e \rightarrow p$ . In the following, without further specification, all discussions and calculations apply to a bound system of electrons and protons with an effective electron mass  $m_e^{\text{eff}} = m_p + m_e$ . Note that for  $\gamma_e \approx \gamma_p$  the accelerated protons' energy  $\gamma_p m_p$  is  $\mathcal{O}[(m_p/m_e)]$  larger than the accelerated electrons' energy  $\gamma_e m_e$ .

These speculations and approximations in the one-dimensional model are used only to qualitatively gain some insights into the Compton-rocket accelerations of electrons and protons in an opaque fluid of photons and pairs. Numerical simulations are necessary.

## 5 Luminosities of UHE particles and blackbody radiation

The accelerated electrons and protons reach ultra-high energies and stream out of the halo, carrying away the halo energy of photons and pairs. We calculate their luminosity

and time variation, which can be relevant for observations. Assuming that the halo energy is large and the luminosity is small, we regard the halo as a steady state, like an energy reservoir. The thermal equilibrium is approximately maintained. The energy transfer and temperature cooling are adiabatic. The halo decays and shrinks slowly.

### 5.1 Blackbody radiation luminosity and MeV annihilation line

Due to the large opacity and temperature gradient in the centre of the fluid halo ( $r_+ < r < 2r_+$ ), internal photons diffuse outwards in the radial direction. At the fluid halo outer boundary  $r = 2r_+$ , where the temperature is about  $2m_e$  and pair annihilation occurs, it becomes optically thin, and photons stream out as a continuous blackbody radiation of the characteristic temperature  $2m_e$ . One obtains the blackbody luminosity by solving the radiation transfer (photon diffusion) equation [31],

$$L_\gamma^0 \sim 4\pi(2r_+)^2 \sigma_{\text{SB}} d_f (T_\gamma^+)^4 c \left( \frac{\xi_\gamma}{2r_+} \right) \approx 4 \left( \frac{\xi_\gamma}{2r_+} \right) L_\gamma^+. \quad (5.1)$$

The continuous radiation time scale is

$$\frac{E_\gamma}{L_\gamma^0} \approx \left( \frac{1}{4\eta} \right) \left( \frac{\delta\ell}{c} \right) \left( \frac{2r_+}{\xi_\gamma} \right), \quad (5.2)$$

where the photon luminosity  $L_\gamma^+ = \eta L_{\text{pl}}$  (2.4) and mean-free path  $\xi_\gamma \sim 10^{-4} \lambda_e$  (Fig. 3) are inside the centre of the fluid halo of photons and pairs. In this case, the small screen factor  $\xi_\gamma/2r_+ \sim 8.3 \times 10^{-22}$  is small for the halo size  $\sim 2r_+$  (2.3). The blackbody radiation luminosity (5.1) is a constant  $L_\gamma^0 \sim 10^{-22} L_{\text{pl}}$ , and the time scale (5.2) is large. These values depend on the halo parameters (2.3), (2.4) and (2.9).

This emission is analogous to the blackbody radiation from the Sun's surface. To compare and contrast, we mention the Sun's surface halo of the temperature  $\sim 6 \times 10^3 C^\circ \approx 0.55 \text{ eV}$  and the radius  $6.96 \times 10^{10} \text{ cm}$ , where electrons are not relativistic ( $\langle \gamma_e \rangle \approx 1$ ) and their densities are much smaller than the horizon halo under discussion. The Sun's luminosity is  $L_\odot = 3.83 \times 10^{33} \text{ ergs/sec} \approx 10^{-27} L_{\text{pl}}$ . Thermal photons diffuse from the Sun's core at the temperature  $T_\odot = 15 \times 10^6 C^\circ = 1.5 \times 10^4 \text{ eV} = 3 \times 10^{-2} m_e$ . While in the horizon halo case, the blackbody has a characteristic temperature  $\sim 2m_e$ . Moreover, the radiation spectrum contains the electron-positron annihilation line and reheating of temperature increment  $(11/4)^{1/3}$  before and after annihilation around  $2m_e \approx 1 \text{ MeV}$  [21].

### 5.2 UHE emission luminosity and energy spectrum

Section 4 shows that the KN cross section (4.1) decreases as accelerated electron and proton energies increase. Therefore, we expect high-energy electrons to stream out and carry away the halo energy  $E_\gamma$  of photons and pairs. Using the rates of radiation energy transfer to an accelerated electron and proton pair (4.26), total bulk electron number  $\bar{N}_e = B N_\gamma$  (3.3) and photon-pair number  $N_\gamma$  (2.10), we obtain the luminosity

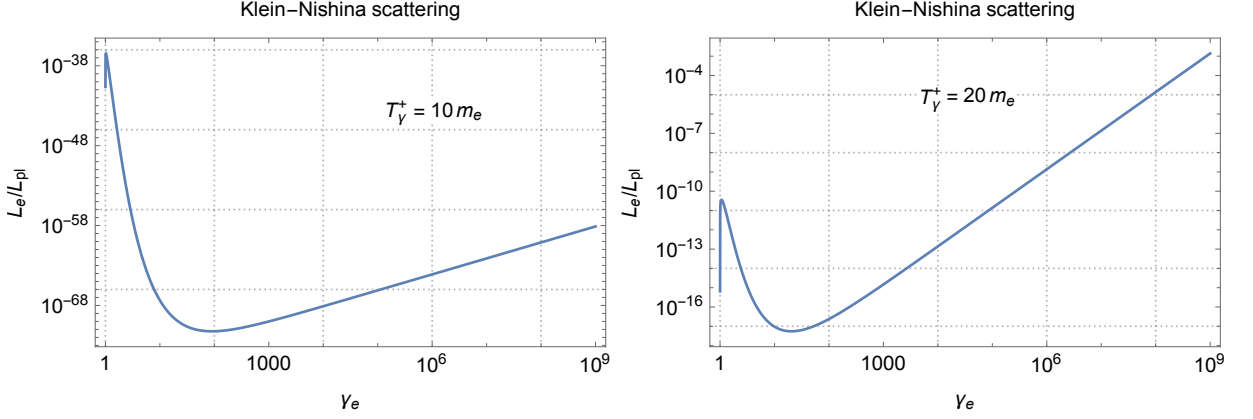


**Figure 6.** For the purpose of illustrating the spectral behaviour of UHE particle luminosity, we select the horizon temperature  $T_\gamma^+ = 10m_e, 20m_e$  and acceleration number  $A = 10^{-3}$ , to plot high-energy electron and proton luminosities  $L_e/L_{\text{pl}}$  (5.3) in terms of their Lorentz factor  $\gamma_e$ .

of high-energy electrons and protons of the Lorentz factor  $\gamma_e$ ,

$$\begin{aligned} L_e &= \frac{dE_e}{dt} \approx N_e \sigma_T F_\gamma(r_+) [(4/3)(\beta_e \gamma_e)^2] \\ &= A \left( \frac{N_e}{\bar{N}_e} \right) \left( \frac{n_\gamma^+}{m_e^3} \right) (4/3)(\beta_e \gamma_e)^2 L_\gamma^+, \end{aligned} \quad (5.3)$$

where the “acceleration number” is defined as

$$A = B(\sigma_T \delta \ell m_e^3), \quad (5.4)$$

indicating the effective number of bulk electrons  $\bar{N}_e$  accelerated inside the volume  $(\sigma_T \delta \ell)$  of one-dimensional tube of photon-electron interactions. We treat the  $A$  as a parameter, depending on the  $B \ll 1$  and  $(\sigma_T \delta \ell m_e^3) = (8\pi/3)\alpha^2(\delta \ell/\lambda_e)$ , which can be much larger than one.

We point out that the obtained UHE emission luminosity (5.3) exhibits three distinct features:

- (1) The luminosity sensitively depends on the horizon temperature  $T_\gamma^+$  (2.9), via the photons and pairs number density  $n_\gamma^+ \equiv n_\gamma(T_\gamma^+)$  (2.8) and the fraction  $(N_e/\bar{N}_e)$  (4.15) of electrons accelerated up to the Lorentz factor  $\gamma_e$ . Figure 5 shows that the fraction  $N_e/\bar{N}_e$  is exponentially suppressed by small temperatures  $T_\gamma^+ \lesssim 10m_e$ , therefore, the UHE emission luminosity (5.3) is completely negligible in this case, unless the non-trivial acceleration number  $A \gg 1$  (5.4), which relates to the baryon-loading  $B$  and size  $\delta \ell$  of the horizon halos (spots) of energetic photons and pairs.
- (2) The fraction  $N_e/\bar{N}_e$  properties (4.16) and Figure 5 imply the UHE emission luminosity (5.3) of particles' energies  $m_e^{\text{eff}} \gamma_e$  follows the spectral behaviour

$$(i) L_e \propto (\gamma_e)^{2-\nu}, \quad (\gamma_e < 10^3); \quad (ii) L_e \propto (\gamma_e)^2, \quad (\gamma_e > 10^3), \quad (5.5)$$

as shown in Fig. 6. This is consistent with the Compton-rocket effect (3.1) and (3.2) [5], which states that relativistic electrons gain more energy ( $\gamma_e > 1$ ) from radiation photons than non-relativistic ones ( $\gamma_e \approx 1$ ).

- (3) Similar to the blackbody radiation (5.1), the UHE emission is not a transient phenomenon, but rather a lasting, continuous radiation, although the luminosity increases with the UHE particles' energy  $m_e^{\text{eff}} \gamma_e$ . The reason is that the fraction ( $N_e/\bar{N}_e$ ) becomes tiny, and the emission time scale

$$\frac{E_\gamma}{L_e} \approx \left( \frac{\delta \ell}{c} \right) \left[ A \left( \frac{N_e}{\bar{N}_e} \right) \left( \frac{n_\gamma^+}{m_e^3} \right) (4/3) (\beta_e \gamma_e)^2 \eta \right]^{-1}, \quad (5.6)$$

becomes even larger than the blackbody one (5.2).

For the second point (2), the increment luminosity  $L_e \propto (\gamma_e)^2$  with  $\gamma_e$  does not run to infinity  $L_e \propto (\gamma_e)^2 \rightarrow \infty$  in time. The reason is that the large luminosity  $L_e$  decreases the halo temperature  $T_\gamma^+$  and energy  $E_\gamma$  faster in time, as required by total energy conservation. As a result, the accelerated electron fraction  $N_e/\bar{N}_e$  (4.17) and the UHE emission luminosity  $L_e$  (5.3) of large  $\gamma_e$  decreases fast in time, as will be shown below.

To compare two emission processes from the horizon halo, we calculate the ratio of the blackbody radiation (5.1) and UHE emission (5.3) luminosities given by

$$\frac{L_e}{L_\gamma^0} = A \left( \frac{N_e}{\bar{N}_e} \right) \left( \frac{n_\gamma^+}{m_e^3} \right) (\beta_e \gamma_e)^2 \left( \frac{\xi_\gamma}{2r_+} \right)^{-1}. \quad (5.7)$$

There are two possibilities: (i) the blackbody radiation is dominant  $L_e/L_\gamma^0 \ll 1$  for small temperature  $T_\gamma^+ \gtrsim m_e$  and fraction  $N_e/\bar{N}_e \ll 1$ ; (ii) the UHE emission is dominant  $L_e/L_\gamma^0 \gg 1$  for large temperature  $T_\gamma^+ \gg m_e$  and the fraction  $N_e/\bar{N}_e$  is significant non-trivial. The former case is well studied, and the blackbody luminosity is small due to the halo's large opacity ( $r_+/\xi_\gamma \gg 1$ ). We are primarily interested in the latter case for  $\gamma_e \gg 1$ , when  $T_\gamma^+ \gg m_e$  and the UHE emission dominantly dissipates the energy  $E_\gamma$  (2.5) of the horizon halo.

### 5.3 UHE emission luminosity and halo temperature decrease in time

The blackbody emission (5.1) and the UHE emission (5.3) dissipate the halo thermal energy  $E_\gamma$  (2.5), therefore, the energy conservation yields

$$-\frac{dE_\gamma}{dt} = \frac{dE_\gamma^0}{dt} + \frac{dE_e}{dt} = L_\gamma^0 + L_e. \quad (5.8)$$

We use this equation together with Eqs. (2.5), (5.3) and (5.7) to determine how the horizon temperature  $T_\gamma^+(t)$  decreases in time,

$$\begin{aligned} \frac{dT_\gamma^+(t)}{dt} &= -1.23B \left( \frac{N_e}{\bar{N}_e} \right) \left( \frac{\sigma_T}{4\pi r_+^2} \right) (\beta_e \gamma_e)^2 L_\gamma^+ \left( 1 + \frac{L_\gamma^0}{L_e} \right) \\ &= -10.4\eta A \left( \frac{N_e}{\bar{N}_e} \right) (\beta_e \gamma_e)^2 m_e^2 \left( 1 + \frac{L_\gamma^0}{L_e} \right), \end{aligned} \quad (5.9)$$

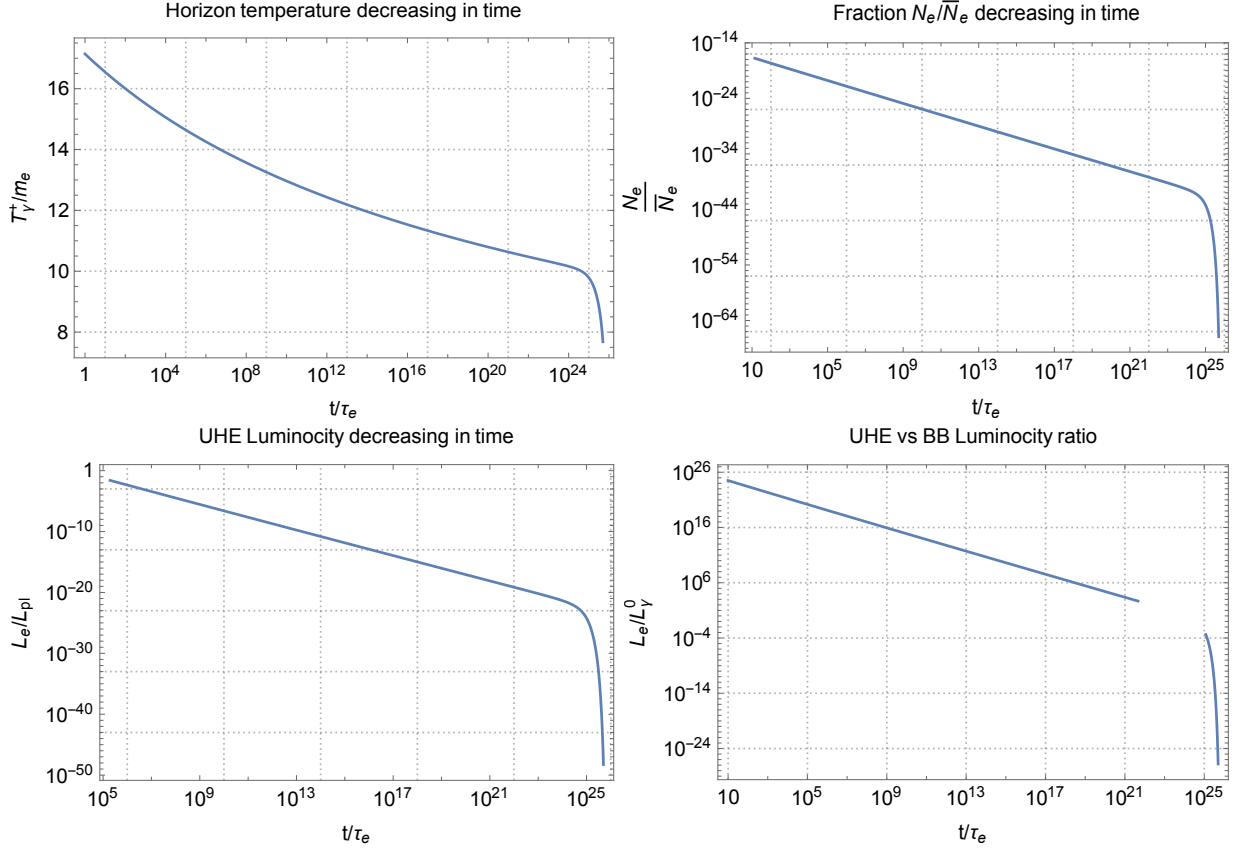


**Figure 7.** For illustrating the numerical results, we adopt the initial horizon temperature  $T_\gamma^+(0) = 100m_e \approx 50$  MeV (2.9) and the collision number  $A = 10^{-3}$  (5.4). We consider the Lorentz factor  $\gamma_e \sim 10^9$  channel, corresponding to UHE electron energies  $\sim 10^3$  TeV and proton energies  $\sim 10^3$  PeV. The Compton time  $\tau_e = (\lambda_e/c) = 1.28 \times 10^{-21}$  sec, and the final time  $10^{26}\tau_e$  is about days. The  $L_e/L_\gamma^0$  broken line (log-log plot) indicates the transition tuning place from the UEH emission dominant  $L_e/L_\gamma^0 \gg 1$  to the blackbody (BB) emission dominant  $L_e/L_\gamma^0 \ll 1$ . For different values of  $\gamma_e$  and  $T_\gamma^+(0)$ , the results will exhibit the same behaviours in time variations. The UHE emission luminosity  $L_e$  will increase for large initial temperature  $T_\gamma^+(0)$  and acceleration number  $A$ , and the emission will last longer for smaller  $\gamma_e$  channels of UHE particles.

where the factor  $\eta$  in the second line comes from the boundary condition (2.3). In the halo decay equation (5.9), we particularly consider a large  $\gamma_e \gg 1$  channel, because it dominates the energy dissipation of the horizon halo. Before presenting numerical calculations, we note that in the luminosities  $L_\gamma^0$  (5.1) and  $L_e$  (5.3), and  $dT_\gamma^+/dt$  (5.9), the gravitational redshift in energy and the gravitational dilation in time are simplified.

For a given  $\gamma_e \gg 1$  value and an initial value  $T_\gamma^+(0)$  at the time  $t = 0$ , we use the numerical result  $N_e/\bar{N}_e$  (4.15) as a function of  $T_\gamma^+(t)$  to integrate the halo decay equation (5.9) over the time. Furthermore, substituting the numerical solution  $T_\gamma^+(t)/m_e$  into  $(N_e/\bar{N}_e)$  and  $(n_\gamma^+/m_e^3)$  in Eq. (5.3), we calculate the UHE emission luminosity  $L_e(t)$  declining as a function of the time  $t/\tau_e$ . Although complex, we calculate the numerical

integrations using the program in Mathematics. Figure 7 shows that the numerical results of the horizon temperature  $T_\gamma^+(t)/m_e$ , accelerated electron fraction  $N_e(t)/\bar{N}_e$ , and the UHE emission luminosity  $L_e(t)$  monotonically decrease in the time  $t/\tau_e$  varying up to  $10^{26}\tau_e$ , which is about days. The results show two phases. (i) The initial phase: the UHE emission initially dominates over the blackbody radiation  $L_e/L_\gamma^0 > 1$ , and the turning point to  $L_e/L_\gamma^0 < 1$  occurs around  $t = 10^{25}\tau_e$  when  $T_\gamma^+ \approx 10m_e$ , and  $N_e(t)/\bar{N}_e$  drops significantly. (ii) The later phase: the horizon halo cooling process attributed to the blackbody radiation  $L_\gamma^0$  (5.1) and the temperature  $T_\gamma^+$  drops at a different slope from that in the initial phase.

In the UHE emission luminosity dominant phase  $L_e/L_\gamma^0 \gg 1$ , we neglect the small time-variation effect of the blackbody luminosity  $L_\gamma^0(t)$  (5.1) caused by the time varying mean-free path  $\xi_\gamma = (\sigma_\gamma n_\gamma^+)^{-1}$  (2.7) and number density  $n_\gamma^+ \propto [T_\gamma^+(t)/m_e]^3$ . The effect should probably be considered in the blackbody luminosity  $L_e/L_\gamma^0 \ll 1$  dominant phase, when the horizon temperature  $T_\gamma^+ < 10m_e$ , electron-positron pair annihilation into two photons occurs and the halo opacity drops. As a consequence, the TOV equilibrium (2.2) is lost and the horizon halo (or spot) shrinks and disappears. These are not the topics of this study and will be subjects of future investigations.

We adopt a simplified model to study the acceleration processes of UHE electrons and protons. These processes occur when a fireball (spot) forms during gravitational processes of accretion, collapse and coalescence. The entire process is complex, and numerical studies are required.

## 6 Characteristics relevant for observations and experiments

### 6.1 Peculiar features of the mechanism accelerating UHE particles

Based on a trapped fireshell halo around the horizon, the Compton-rocket effect, and unstable runaway dynamics, we qualitatively discuss a possible microscopic mechanism for producing UHE particles (electrons and protons) in the opaque, high-temperature fluid of photons and pairs, which can form in high-energy astrophysical processes and environments. Discussions and calculations are in an idealised one-dimensional model. Nevertheless, we highlight some qualitative characteristics of this mechanism:

- (1) The mechanism occurs at local microscopic length and time scales, over which the photon-pair fluid temperature ( $T_\gamma \gg m_e$ ) has a large gradient, resulting in a strong radiation force for electron and proton acceleration. Therefore, the mechanism does not essentially depend on the global symmetry, macroscopic length and time scales of high-energy astrophysical environments and strong gravitational processes, which create such a fire spot of highly dense and energetic fluid of photons and pairs. Therefore, the trapped fireshell (spherical halo) near the horizon is only an example for simplifying calculations and illustrations. The fire spots can be formed, for instance, in gravitational binary coalescence and accretion cases, and may be in future laser experiments.
- (2) The horizon temperature  $T_\gamma^+ > 10m_e$ , as if an effective overcritical classical electric field  $E_{\text{eff}} \sim \mathcal{O}(10)E_c$ , provides a significant probability of accelerating electrons and



protons to UHE up to TeV, PeV, EeV scales and even higher. The total luminosity of UHE particles increases as the acceleration number  $A$  increases, namely, more electrons in the fireshell participate in the acceleration process. The UHE particle luminosity (5.3) could be significant for the small temperature  $2m_e < T_\gamma^+ < 10m_e$  and the large acceleration number  $A$ . However, we cannot show the results, because the numerical precision is limited in calculating the exponential factor  $e^{-m_{\text{eff}}/T_\gamma^+}$ .

- (3) The UHE emission is not a transient burst, but a long-lasting continuous radiation. The luminosity of UHE particles has a peculiar spectral behaviour: an approximate power law  $\gamma_e^{-\nu}$  for  $\gamma_e \lesssim 10^3$ , and being proportional to  $\gamma_e^2$  for  $\gamma_e \gtrsim 10^3$ . For the appropriate values of the photon and pair temperature  $T_\gamma^+ > 10m_e$  and acceleration number  $A$ , the resultant UHE emission luminosity (emission probability) and energy spectra (Lorentz factor  $\gamma_e$  or  $\gamma_p$ ) can be relevant for observations.

UHE electrons and protons interact with fields and particles in the medium around their sources, producing VHE photons and neutrinos. Since these interactions are highly energetically forward scattering, resultant secondary VHE particles carry the characteristics of initial primary UHE particles. Therefore, the characteristics (1)-(3) in terms of only two basic parameters  $T_\gamma^+$  and  $A$  can be relevant for verification or falsification by the observations of UHE and VHE particles.

## 6.2 Possible relevance for observations and experiments

In this article, we focus only on revealing the novel scenario and mechanism of generating UHE particles, and pay no attention to quantitatively discussing this scenario compared with the observations of UHE and VHE particles. Nevertheless, we mention some observationally and experimentally relevant features below:

- (1) Interacting with magnetic fields, soft photons and other low-energy particles around sources, these UHE electrons and protons from the opaque fluid spot of highly energetic photons and pairs produce VHE photons and neutrinos to TeV or PeV energy scales. In addition to astrophysical sources, such an energetic spot would be created in future by strong laser-beam experiments. The probability of producing UHE particles could be non-trivial for detection, if the strong laser field spot is not only sufficiently energetic  $T_\gamma \gg m_e$  and dense  $A \gg 1$ , but also has a lifetime longer than the time scale  $\tau_{\text{KN}}^e = (\sigma_{\text{KN}}^e n_\gamma c)^{-1}$  (4.2) for the runaway process.
- (2) We come to the GRBs' cases. As shown in Fig. 7, the trapped fireballs (horizon halos) cool via continuous emission of UHE electrons and protons. Interacting with the surrounding fields and materials, the former mainly leads to VHE photons, and the latter to VHE neutrinos. Before outward expanding fireballs become optically thin, we probably cannot see VHE photons because of great opacity due to two-photon annihilation  $\gamma\gamma \rightarrow e^+e^-$  of the Breit-Wheeler process (2.6). It strongly implies that the VHE photons most probably observed are after expanding fireballs become transparent, namely, VHE photon luminosity increases soon after the main GRBs' bursts [24]. During the afterglow era, UHE protons  $\gamma_p \gg 1$



emitted from the horizon halo continuously collide with the ejector of the Lorentz factor  $\Gamma < \gamma_p$ , which then emits VHE photons and neutrinos. Therefore, their light curves follow the law of the ejector's kinematic motion in time, similarly to the external shock emission of the ejector colliding with the interstellar medium. However, their energy spectra become softer in time because the horizon halos cool down. The time and luminosity of UHE and VHE continuous emissions depend on the horizon-halo temperature  $T_\gamma$  and acceleration number  $A$ , as well as the target (ejector) density.

- (3) The scenario and mechanism in principle apply to the early Universe at large particle density and high temperature  $T_\gamma > 2m_e$  before the Universe becomes transparent. Local dense and inhomogeneous radiation fields accelerate charged particles to high energies. It implies that in the cosmic background observed today, there should be imprints of excess UHE and VHE particles originating from the early Universe.

Further investigations in theoretical studies, numerical simulations, observations and experiments are necessary in future.

## References

- [1] N. Globus and R.D. Blandford, *Ultrahigh-energy cosmic rays*, *Annual Reviews of Astronomy and Astrophysics* **63** (2025) 339 [[2505.21846](#)].
- [2] Z. Cao and others (LHAASO collaboration), *Ultrahigh-energy photons up to 1.4 petaelectronvolts from 12  $\gamma$ -ray Galactic sources*, *Nature* **594** (2021) 33.
- [3] MAGIC collaboration, *Teraelectronvolt emission from the  $\gamma$ -ray burst grb 190114c*, *Nature* **575** (2019) 455 [[2006.07249](#)].
- [4] ICECUBE collaboration, *Observation of high-energy neutrinos from the Galactic plane*, *Science* **380** (2023) 9818 [[2307.04427](#)].
- [5] S.L. O'Dell, *Radiation force on a relativistic plasma and the Eddington limit*, *Astrophys. J. Lett.* **243** (1981) L147.
- [6] M. Sikora, *Superluminous accretion discs*, *Mon. Not. R. Astron. Soc.* **196** (1981) 257.
- [7] E.S. Phinney, *Acceleration of a relativistic plasma by radiation pressure*, *Mon. Not. R. Astron. Soc.* **198** (1982) 1109.
- [8] J.T. Frederiksen, *Stochastically induced gamma-ray burst wakefield processes*, *The Astrophysical Journal* **680** (2008) L5.
- [9] F. Del Gaudio, R.A. Fonseca, L.O. Silva and T. Grismayer, *Plasma wakes driven by photon bursts via compton scattering*, *Phys. Rev. Lett.* **125** (2020) 265001 [[2003.04249](#)].

- [10] B. Martinez, T. Grismayer and L.O. Silva, *Compton-driven beam formation and magnetization via plasma microinstabilities*, *J. Plasma Phys.* **87** (2021) 905870313 [[2102.11590](#)].
- [11] J.C. Faure, D. Tordeux, L. Gremillet and M. Lemoine, *High-energy acceleration phenomena in extreme-radiation-plasma interactions*, *Phys. Rev. E* **109** (2024) 015203 [[2309.00366](#)].
- [12] M.J. Rees and P. Meszaros, *Relativistic fireballs - energy conversion and time-scales*, *Mon. Not. Roy. Astron. Soc.* **258** (1992) 41.
- [13] T. Piran, *The physics of gamma-ray bursts*, *Reviews of Modern Physics* **76** (2004) 1143 [[astro-ph/0405503](#)].
- [14] P. Mészáros, *Gamma-ray bursts*, *Reports on Progress in Physics* **69** (2006) 2259 [[astro-ph/0605208](#)].
- [15] E. Berger, *Short-Duration Gamma-Ray Bursts*, *Annual Review of Astron and Astrophys* **52** (2014) 43 [[1311.2603](#)].
- [16] P. D’Avanzo, *Short gamma-ray bursts: A review*, *Journal of High Energy Astrophysics* **7** (2015) 73.
- [17] P. Kumar and B. Zhang, *The physics of gamma-ray bursts & relativistic jets*, *Physics Reports* **561** (2015) 1 [[1410.0679](#)].
- [18] B. Zhang, *The Physics of Gamma-Ray Bursts*, Cambridge University Press (2018), [10.1017/9781139226530](#).
- [19] R. Ruffini, G. Vereshchagin and S.-S. Xue, *Electron-positron pairs in physics and astrophysics: from heavy nuclei to black holes*, *Phys. Rept.* **487** (2010) 1 [[0910.0974](#)].
- [20] C. Kouveliotou, R.A.M.J. Wijers and S. Woosley, *Gamma-ray Bursts*, Cambridge University Press (2012).
- [21] R. Ruffini, J.D. Salmonson, J.R. Wilson and S.-S. Xue, *On the pair electromagnetic pulse of a black hole with electromagnetic structure*, *Astron. Astrophys.* **350** (1999) 334 [[astro-ph/9907030](#)].
- [22] R. Ruffini, J.D. Salmonson, J.R. Wilson and S.-S. Xue, *On the pair-electromagnetic pulse from an electromagnetic black hole surrounded by a baryonic remnant*, *Astron. Astrophys.* **359** (2000) 855 [[astro-ph/0004257](#)].
- [23] R. Ruffini, L. Vitagliano and S.-S. Xue, *On a separatrix in the gravitational collapse to an overcritical electromagnetic black hole*, *Phys. Lett. B* **573** (2003) 33 [[astro-ph/0309022](#)].
- [24] S.-S. Xue, *Gravo-thermal catastrophe in gravitational collapse and energy progenitor of Gamma-Ray Bursts*, *JCAP* **07** (2021) 044 [[2104.03021](#)].

- [25] S.-S. Xue, *Collimated and spinning fireballs for ultra-relativistic jets: long vs short gamma-ray bursts by angular momentum and mass ratio*, *Eur. Phys. J. C* **85** (2025) 820 [[2406.00454](#)].
- [26] Y.-B. Wu and S.-S. Xue, *Nonlinear Breit-Wheeler process in the collision of a photon with two plane waves*, *Phys. Rev. D* **90** (2014) 013009 [[1403.4798](#)].
- [27] B. Zhang, Z.-M. Zhang, Z.-G. Deng, W. Hong, J. Teng, S.-K. He et al., *Effects of Involved Laser Photons on Radiation and Electron-Positron Pair Production in one Coherence Interval in Ultra Intense Lasers*, *Sci. Rep.* **8** (2018) 16862.
- [28] B. Zhang, Z. Zhang, Z.-g. Deng, J. Teng, S.-K. He, W. Hong et al., *Quantum mechanisms of electron and positron acceleration through nonlinear Compton scatterings and nonlinear Breit-Wheeler processes in coherent photon-dominated regime*, *Scientific Reports* **9** (2019) 18876.
- [29] X. Xu, P. Yu, S.F. Martins, F.S. Tsung, V.K. Decyk, J. Vieira et al., *Numerical instability due to relativistic plasma drift in EM-PIC simulations*, *Computer Physics Communications* **184** (2013) 2503 [[1211.0953](#)].
- [30] G.R. Blumenthal, *The Poynting-Robertson Effect and Eddington Limit for Electrons Scattering with Hard Photons*, *Astrophys. J.* **188** (1974) 121.
- [31] E. Böhm-Vitense, *Introduction to Stellar Astrophysics: Volume 3*, Introduction to Stellar Astrophysics, Cambridge University Press (1989).